POLITECNICO DI TORINO
Repository ISTITUZIONALE

Comparison of Induction and PM Synchronous motor drives for EV application including design examples

Original
Comparison of Induction and PM Synchronous motor drives for EV application including design examples / Pellegrino, G.-.M.L., Vagati, A., Boazzo, B., Guglielmi, P.. - In: IEEE TRANSACTIONS ON INDUSTRY APPLICATIONS. - ISSN 0093-9994. - STAMPA. - 48:6(2012), pp. 2322-2332. [10.1109/TIA.2012.2227092]

Availability:
This version is available at: 11583/2503176 since:

Publisher:
IEEE

Published
DOI:10.1109/TIA.2012.2227092

Terms of use:

This article is made available under terms and conditions as specified in the corresponding bibliographic description in the repository

Publisher copyright

(Article begins on next page)

01 November 2026

Comparison of Induction and PM Synchronous motor drives for EV application including design examples

Gianmario Pellegrino, Alfredo Vagati, Barbara Boazzo and Paolo Guglielmi
Politecnico di Torino, Corso Duca degli Abruzzi 24, Torino, 10129 Italy
gianmario.pellegrino@polito.it

***Abstract* -- Three different motor drives for electric traction are compared, in terms of output power and efficiency at same stack dimensions and inverter size. Induction motor, surface mounted permanent magnet (SPM) and interior permanent magnet (IPM) synchronous motor drives are investigated, with reference to a common vehicle specification. The induction motor is penalized by the cage loss but it is less expensive and inherently safe in case of inverter unwilled turn-off due to natural de-excitation. The SPM motor has a simple construction and shorter end-connections, but it is penalized by eddy current loss at high speed, has a very limited transient overload power and has a high uncontrolled generator voltage. The IPM motor shows the better performance compromise, but it might be the more complicated to be manufactured. Analytical relationships are first introduced and then validated on three example designs, Finite-Element calculated, accounting for core saturation, harmonic losses, the effects of skewing and operating temperature. The merits and limitations of the three solutions are quantified comprehensively and summarized by calculation of the energy consumption over the standard NEDC driving cycle.**

Index Terms* -- *Permanent magnet machines, Variable Speed Drives, Synchronous Motor Drives, Induction Motor Drives, Traction Motor Drives, Electric Machine Design Comparison.

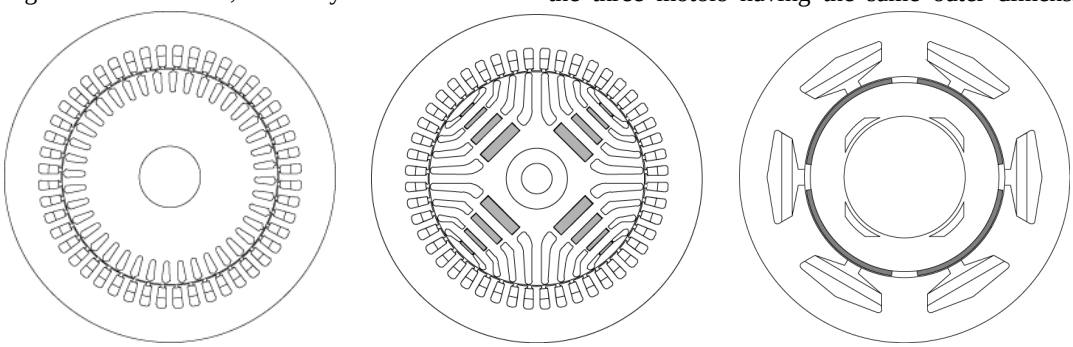
I. INTRODUCTION

State of the art drive trains for Electric Vehicles (EVs) are often equipped with induction motors (IM) or permanent magnet (PM) synchronous motors [1,2]. IM drives are adopted for their ruggedness and universal availability. Also on the control side, field-oriented vector control of IMs is considered a standard, industrially. Moreover, IMs are naturally de-excited in case of inverter fault and this is very welcome among car manufacturers, for safety reasons.

Permanent Magnet motor drives are considered to have a higher torque density and efficiency, with respect to IMs. Among PM motors, both surface-mounted PM (SPM) and interior PM (IPM) types are adopted for traction [3]. SPM motors for traction have concentrated stator coils [4], that is very short end connections and an easier stator construction. They suffer from eddy current loss in the PMs at high speed and need structural sleeves for PM retention. Arc magnets such as the ones in Fig. 1c can be a problem industrial-wise, but different rotor solutions are possible, also contributing to mitigate PM loss [18]. IPM motors require rotors with multiple flux barriers for having a high saliency, such as the one in Fig. 1b, that might look complicated industrial-wise. However the high saliency is synonymous of a much larger overload torque over the entire speed range [5], a safer back-emf in uncontrolled generator operation [6] and little sensitivity to PM temperature.

Synchronous PM drives of both types require a custom control algorithm, when flux-weakening operation is required over a wide speed range, as it is the case of traction. The motor magnetic model must be consistently identified for accurate control, with the experimental identification tests that are considered cumbersome if compared to the standard ones, usual for IMs. The recent issue of the rare-earth magnets price volatility is seriously questioning the adoption of PM motor drives [7]. In this scenario, multi-layer IPM motors are more suitable for replacing the rare-earth magnets with cheaper ferrite magnets, at least in some cases [9], while SPM and single layer IPMs are not.

The comparison between IM, SPM and IPM motor drives for EVs is proposed, at a given vehicle specification and with the three motors having the same outer dimensions of the



(IM) (IPM) (SPM)

Figure 1. Induction motor, Interior PM motor and Surface mounted PM motor under investigation.

active parts (stack diameter and length) and the same inverter size (maximum voltage and current). The paper extends the comparison of [5] to include the asynchronous motor, giving further insights on aspects such as skewing and PM temperature.

Three example motors are designed and FEA characterized. Their laminations are represented in Fig. 1. Unfortunately, it was not possible to build and test three prototypes to be experimentally compared. However, finite element simulation can still be considered a consistent instrument of virtual prototyping of electrical machines, accepted industrial-wise, as documented in the literature [12,20,21], also for loss evaluation [22].

II. Terms of the Comparison

A. Vehicle specification

As summarized in Fig. 2, EVs require a constant-torque operating region at low speed for starting and up-hill march and then a constant power speed range at higher vehicle speed. The continuous power at maximum speed P_1 determines the maximum speed of the vehicle on flat (***F*** red square, for *Flat*). The continuous stall torque T_1 determines the maximum slope that the vehicle can climb continuously (***U*** red square, for *Uphill*). Transient overload torque and power are limited by the inverter current rating (i_0), and the combination of voltage and current limits (v_0, i_0), respectively. The typical areas of urban and extra-urban operations are also evidenced in Fig. 2, that will be calculated according to the NEDC driving cycle for the final designs of section VII. ECE15 and EUDC in Fig. 2 indicate urban and extra-urban, according to the NEDC standard [23]. Detailed vehicle specifications are reported in the Appendix.

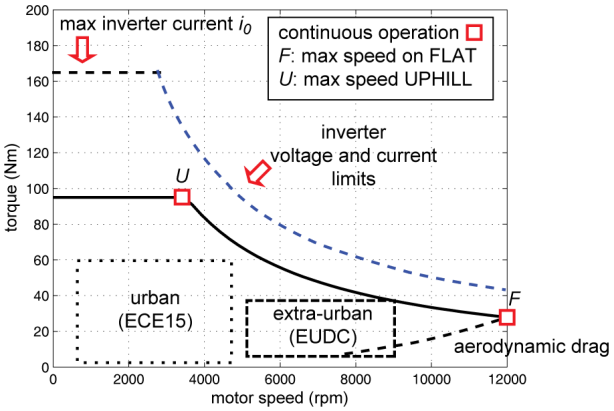


Figure 2. Example of target specification for an electric vehicle.

B. Common data and goals of the comparison

The torque versus speed profiles of Fig. 2 are indicative but not mandatory, except for point *F*: the three drives under comparison must comply with ***the basic requirement of giving the same maximum vehicle speed***, that is giving the same continuous power at the maximum motor speed of 12000 rpm. All the other parameters evidenced in Fig. 2 are matter of the comparison: continuous torque at point *U*, maximum overload torque at given inverter current, transient overload, efficiency over the whole operation area and in the preferred maximum efficiency area. The stack outside diameter, stack length and airgap length are the same for the three motors, as well as the same liquid cooling setup. It is assumed that the stator windings are at 130 °C in continuous operation, the PMs are at 150 °C and the rotor of the IM at 180 °C. The inverter voltage and current are set to v_0 = 173 Vpk, phase voltage, corresponding to a 300 V dc-link and i_0 = 360 Apk phase current.

III. Induction Motor Drive

A. Motor model in the rotor field oriented frame

The *dq* reference frame, synchronous to the rotor flux is considered. In this frame, the stator flux vector components, at steady-state, become:

$$\begin{cases} \lambda_{sd} = L_s \cdot i_{sd} \\ \lambda_{sq} = \sigma \cdot L_s \cdot i_{sq} \end{cases} \qquad (1)$$

where L_s is the stator self inductance, σ is the total leakage factor (2) and σL_s is the stator transient inductance.

$$\sigma = 1 - \frac{L_M^2}{L_s \cdot L_r} \qquad (2)$$

The steady-state expressions of stator voltage and torque are:

$$\bar{v}_{sdq} = R_s \cdot \bar{i}_{sdq} + j\omega \cdot \bar{\lambda}_{sdq} \qquad (3)$$

$$T = \tfrac{3}{2} \cdot p \cdot \left(\bar{\lambda}_{sdq} \wedge \bar{i}_{sdq} \right) \qquad (4)$$

where ω is the synchronous electrical speed. Last, the slip speed at steady state is:

$$\omega_{sl} = \tau_r^{-1} \cdot \left(\frac{i_{sq}}{i_{sd}} \right) \qquad (5)$$

where $\tau_r = L_r/R_r$ is the rotor time constant and R_r the rotor resistance reported to the stator. Independently of the control technique (rotor field oriented, stator field oriented, direct torque control), the magnetic model (1) can be used in association to (3)-(5) for describing the torque and power curves as a function of rotor speed, at given voltage and current limits [15,16].

B. Power curves at constant current

The stator current and flux linkage vectors will be indicated, from now on, as flux linkage and current, with no subscript *s*, as also for the other motors described in the following sections. The vector trajectories of the IM drive, corresponding to a given current amplitude, with limited voltage, are qualitatively illustrated in Fig. 3, along with the

corresponding power versus speed curves, in Fig. 4. The vector diagrams and power curves are replicated for the continuous current i_1 and for the maximum current i_0. This may be not representative of the actual control trajectories of the drive, but power curves at given voltage and different current limits will be useful here and in the following for comparing the characteristics of the different drives.

It must be underlined that i_0 is the same for all the three drives, that have the same inverter, while i_1 depends on the machine type and will be slightly different for the three motors.

In Fig. 3 the stator current and stator flux linkage vector trajectories are reported [17]. As said, the *d* axis is the direction of the rotor flux linkage vector. At low speed, the MTPA (Maximum Torque Per Ampere) condition is considered, that means the overload point (A') will require a slightly higher d current component, if compared with the rated current point (A). At higher speeds, the voltage limit requires that the current vector is rotated towards the *q* axis (flux weakening region I), until the flux argument becomes 45°, that is the MTPV (Maximum Torque Per Voltage) condition represented as B and B', respectively. From B (and B') on, both current and flux vectors are reduced at constant phase angle (flux weakening region II).

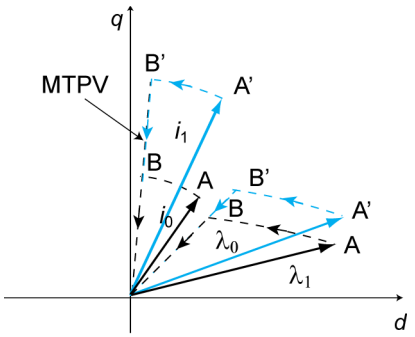


Figure 3. Induction motor current and flux vector trajectories for maximum power under limited voltage amplitude

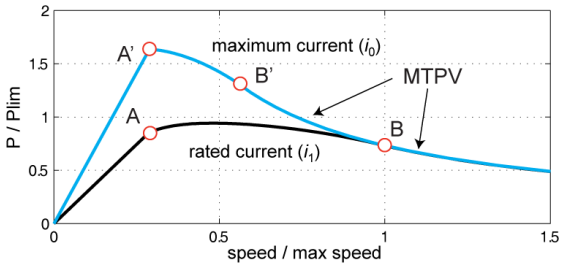


Figure 4. Induction motor power versus speed curves, for rated and overload current amplitudes and limited voltage.

In Fig. 4 the normalized power curves corresponding to rated and overload currents are shown. Unitary speed is the maximum operating speed, while the base power is equal to $P_{lim} = 3/2 \cdot v_0 \cdot i_1$. With this power scale, the A to B region of the power curve at rated current i_1 coincides with the power factor (PF) of the motor, having disregarded the losses. A good design practice is to design a motor having the transient inductance as low as possible, to push the MTPV region at rated current over the maximum speed, or at least not under, as in Fig. 4 (maximum speed is 1 per unit). This approach maximizes the output power at maximum speed, given the inverter size. At overload, B' is at a lower speed than B, how lower depending on the overload ratio i_0/i_1. From point B' on the power curve drops to rejoin the rated current curve at point B.

IV. IPM MOTOR DRIVE

A. *Motor model*

The voltage vector and torque expression are formally identical to the one of the IM, (3) and (4), respectively. The linear magnetic model of the IPM motor is expressed by:

$$\begin{aligned} \lambda_d &= L_d \cdot i_d + \lambda_m \\ \lambda_q &= L_q \cdot i_q \end{aligned} \qquad (6)$$

where λ_m is the PM flux linkage and the *d*, *q* inductance values are different according to the rotor saliency:

$$\xi = \frac{L_q}{L_d} > 1 \qquad (7)$$

Due to magnetic saturation, the two inductances (L_q in particular) are variable with the current vector working point, and also *d*-*q* cross-coupling terms should be included in the magnetic equations (6).

B. *Power curves at constant current*

The vector trajectories and power curves are reported also for the IPM motor drive, in Fig. 5 and 6 respectively [17], for the case of a motor having high anisotropy and low per unit PM flux linkage. In this case, the phase angle of the current vector corresponding to MTPA is leading the *q* axis by 45° or even more [5]: in Fig. 5 point A (rated current) and point A' (maximum current) represent operation below the base speed. After the voltage limit, the current vector is rotated for flux weakening towards the MTPV locus, if any. Synchronous PM drives actually have a MTPV region (flux weakening region II) only for current values that are greater than the characteristic current [10]:

$$\left|\bar{i}\right| > i_{ch} = \frac{\lambda_m}{L_d} \qquad (8)$$

The particular design condition (9) is chosen, where the continuous current equals the motor characteristic current i_{ch} for having an ideally flat power profile at rated current:

$$i_1 = i_{ch} \qquad (9)$$

This implies that the MTPV is met only at overload current (e.g. point B' at maximum current i_0).

In Fig. 6 the power versus speed curves of the IPM motor drive are reported at i_1 and i_0. As for the IM, from base speed

on (point A), the per unit power at i_1 is representative of the power factor, due to the scale factor $P_{lim} = 3/2 \cdot v_0 \cdot i_1$, that refers to i_1. The PF at maximum speed is unitary (dark curve, speed equal to 1), while in the same condition the PF of the IM is lower (0.7 in point B of Fig. 4). Slightly better values are possible for the IM, via the minimization of the transient inductance: the example IM design presented in section VI will actually have a PF of 0.8 at maximum speed. Still, the better power factor of the IPM motor leads to a lower i_1 for the same continuous power, given the inverter voltage.

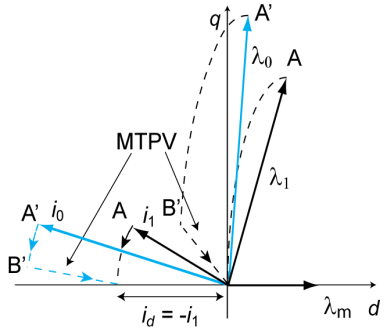


Figure 5. IPM current and flux vector trajectories for maximum power under limited voltage amplitude

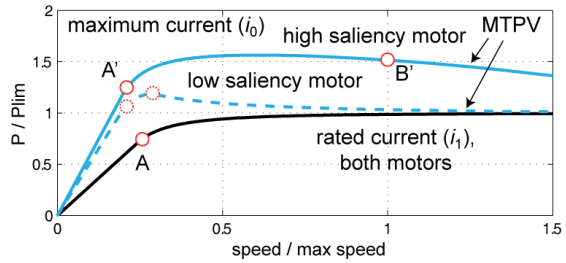


Figure 6. IPM power versus speed curves (limited voltage), for rated and overload current amplitudes. Effect of rotor saliency on the power overload curve:

The power curve at maximum current i_0 is also very flat, due to the high saliency. In Fig. 6 it is also shown, still qualitatively, that a low saliency motor would have a limited power overload capability (dashed overload line), as demonstrated in [5]. Hence, multi-layer IPM rotors like the one in Fig. 1 are more suitable for transient power overload, while less salient structures such as single layer or flux-concentration IPM rotors have the power overload limitations typical of SPM motors, as addressed in the next section.

V. SPM MOTOR DRIVE

A. *Motor model*

The linear magnetic model of the SPM motor is expressed by (6) with $L_d = L_q = L$.

$$\lambda_d = L \cdot i_d + \lambda_m \qquad \lambda_q = L \cdot i_q \qquad (10)$$

The single inductance value for both the *d*, *q* axes is due to the non salient geometry. At a deeper insight, magnetic saturation modifies the two inductances, resulting in magnetic saliency ($L_d \neq L_q$) in spite of the geometry and also produces cross-coupling terms, as for the IPM motor. The voltage and torque expressions are still (3) and (4), respectively, with the latter one becoming very simple when associated to the isotropic model (10):

$$T = \tfrac{3}{2} \cdot p \cdot \lambda_m \cdot i_q \qquad (11)$$

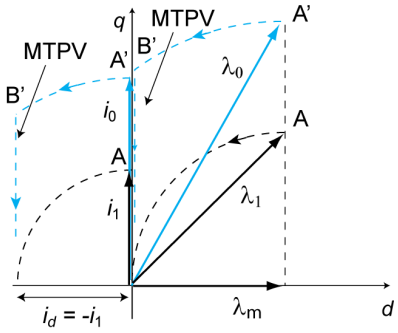


Figure 7. SPM current and flux vector trajectories for maximum power under limited voltage amplitude

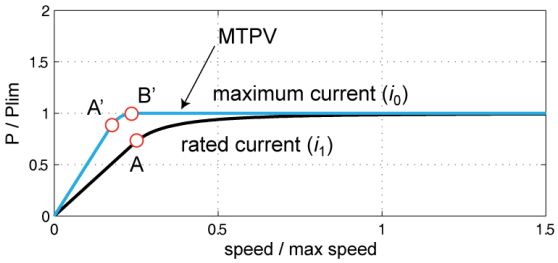


Figure 8. SPM power versus speed curves (limited voltage), for rated and overload current amplitudes

B. *Power curves at constant current*

In Fig. 7 the vector trajectories of the SPM motor drive are reported: at low speed the current vector is along the *q*-axis (points A and A'), that is MTPA operation. At higher speeds, as the voltage limit occurs, the current vector is rotated along the dashed paths for flux weakening. The design condition (9) is chosen also here as for the IPM motor, for the same reason of obtaining a flat power curve at rated current i_1. The MTPV is met when $i_d = -i_{ch} = -i_1$ and the total flux linkage vector is along the *q* axis (point B'). Again, MTPV occurs at overload current only, due to the design condition (9). In MTPV operation the i_d current component remains equal to $-i_{ch}$ and the torque producing component i_q is progressively reduced, as in Fig. 7.

In Fig. 8 the power versus speed curves of the SPM motor drive are reported, for rated and maximum currents. Both the power curves tend asymptotically to one per unit. According to Fig. 7, the flux linkage in MTPV has no *d*-axis component

and it is then directly proportional to torque:

$$\lambda_{MTPV} \equiv \lambda_q = L \cdot i_q = \frac{L}{\frac{3}{2} p \cdot \lambda_m} \cdot T_{MTPV} \quad (12)$$

At high speed, the voltage drop across the stator resistance is negligible:

$$\left|\bar{v}_s\right| \cong \omega \cdot \left|\bar{\lambda}\right| \quad (13)$$

Therefore, from manipulation of (11), (12) and (13) the torque and power at MTPV are obtained.

$$T_{MTPV} = \frac{3}{2} p \cdot \frac{\lambda_m}{L} \cdot \frac{v_0}{\omega} = \frac{3}{2} \cdot \frac{p}{\omega} \cdot i_{ch} \cdot v_0 \quad (14)$$

$$P_{MTPV} = \frac{3}{2} \cdot i_{ch} \cdot v_0 \quad (15)$$

It is then demonstrated that the overload power of SPM motors is upper limited according to the maximum voltage v_0 and the motor characteristic current, ***whatever the available overload current is.*** With the design choice (9), the MTPV power limit coincides with $P_{lim} = 3/2 \cdot v_0 \cdot i_1$, that is the unitary power in Fig. 8.

VI. Design Results and Power Curves

Three example motors having the same active dimensions are designed and compared by means of FEA. The continuous output power specification is 50 kW at 12000 rpm. The inverter voltage is 300 V dc, corresponding to 173 Vpk phase voltage (v_0) and the maximum current (i_0) is 360 Apk. The dimensions of the active stack are: 216 mm stator outside diameter and 170 mm active length for the three motors. The motors are water cooled. The ratings of the cooling setup are discussed in the dedicated subsection VII.F.

The three motors are designed for having the best compromise between continuous power, transient overload power and efficiency. All three are comprehensively evaluated by means of 2D, in terms of magnetic curves, core loss, PM loss and IM cage loss. The magnetic curves are calculated in all the i_d, i_q operating plane, accounting for saturation effects. End connections additional resistance and inductance terms are evaluated analytically, also for the squirrel cage [11]. In particular, the magnetic curves of the IM are precisely evaluated with the method presented in [12]. The motor laminations are the ones reported in Fig. 1. The significant motor ratings are reported in Table I.

All machines have two pole-pairs, for limiting the impact of core and PM losses, given the 12000 rpm operation. The IM and the IPM motor have the same stator laminations, with 48 slots that is 4 slots per pole per phase. Such relatively high number of stator slots helps in minimizing the torque ripple and harmonic core loss of the IPM motor [14]. Dealing with the IM, the 48-40 stator-rotor slot combination of Fig. 1a is one of the suggested ones [24].

A counter-intuitive result of Table I is that the PM quantity of the IPM motor is higher than the one of the SPM: 1.95 kg versus 1.35 kg. This is related to the 12000 rpm speed specification, that results in the IPM rotor having very thick structural ribs in Fig. 1b. The thicker are the ribs, the more of the PM flux is shunted between layer and layer, resulting in an augmented PM quantity. Moreover, the PM quantity could be significantly reduced, as proposed in the recent work [8], and yet not applied to the example machine reported here. Structural ribs have been FEA evaluated against centrifugal stress.

Dealing with the surface mounted PMs, those of Fig. 1c are particularly thin: they have been verified against de-magnetization at 150°C but with PM materials of lower grades they could have problems and should be made thicker. Thicker magnets increase the margin against de-magnetization and re-balance the PM material quantities of the two motors.

TABLE I – RATINGS OF THE THREE MOTOR DESIGNS.

		IM	IPM	SPM
Pole pairs		2		
Stator slots		48		6
Stator outer diameter	mm	216		
Stator bore diameter	mm	142		131
Stack length	mm	170		
Airgap	mm	0.7		
Number of turns		20		23
Copper fill factor		0.4		
End connections (per side)	mm	150		77
Max speed	rpm	12000		
Continuous torque *	Nm	110	160	130
Speed at continuous torque *	rpm	4000	3800	3800
Current at continuous torque	A pk	200	255	294
Maximum speed **	rpm	11300	12000	10300
Overload torque	Nm	210	210	150
Overload current	A pk	360	360	360
Characteristic current (150°C)	A pk		205	193
Phase rated voltage	V pk	173	173	173
Phase back-emf (12000 rpm, 20°C)	V pk		170	540
Stator resistance (130°C)	Ω	0.027	0.027	0.021
Rotor resistance (180°C)	Ω	0.018		
Steel grade		M250–35A		
PM grade			BMN-42SH	
PM mass	kg		1.95	1.35
Rotor temperature		180° C	150° C	150° C

* Low speed dot, in Fig. 13, at 3200 W dissipation

** High speed dot, in Fig. 13, at 3200 W dissipation

A. *Rated power specification*

In Fig. 9 the three example designs are compared in terms of output power at given voltage and current. All three have similar torque for the example current, as the power curves at low speed demonstrate. Dealing with high speed, the SPM and IPM motor drives fulfill the continuous power specification of 50 kW at 12000 rpm with the example current of 216 Apk, that is close to their respective characteristic currents. The IM has a lower output power at high speed and requires a higher current value for the same power. As said, both the PM motors have unitary power factor at high speed with the current around i_{ch} and both their power curves tend to $P_{lim} = 3/2 \cdot v_0 \cdot i_1$, as shown in Figs. 6 and 8, due to the design choice $i_1 = i_{ch}$. Then, for the same output power they have nearly the same characteristic current, as in Fig. 9.The IM has a lower output power at same current and voltage due to the lower power factor, as said in subsection III.B.

B. *Power at maximum inverter current*

The power output at maximum current of the three designs is compared in Fig. 10. As said, the SPM motor has no power overload due to the MTPV power clamping. Moreover, also the torque overload is quite limited with respect to the other two motors, due to hard saturation of the motor core related to the high armature flux at overload, indicated as cross-saturation (the q-current produced flux reduces the d-flux component, that is the torque factor of the machine). The IPM motor and the IM have the same maximum transient overload torque (point A' and speeds below) because, by coincidence, they have exactly the same torque angle at 360 A, MTPA. They both have quite flat power curves. The IPM motor enters the MTPV close to the maximum operating speed and the IM even over the speed rating.

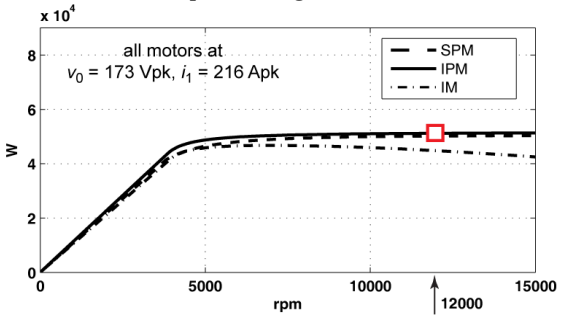


Figure 9. Power curves of the three motors at same current and voltage. SPM and IPM motors fulfill the continuous power specification with the same current and voltage, while the IM requires a higher current.

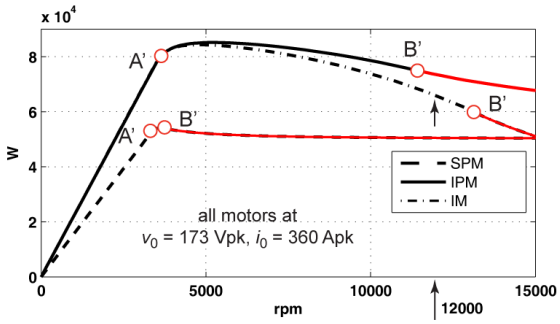


Figure 10. Power curves of the three motors at maximum current and voltage. The continuous red lines, over point B' of the three curves, indicate the MTPV operating region.

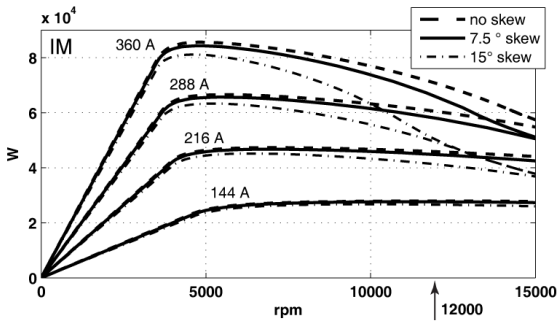
C. *Effect of skewing*

All the three motors are skewed for minimizing torque ripple and possible acoustic noise. The IM and IPM motor have the same stator, with 48 slots, and are both skewed of 7.5 mechanical degrees (one stator slot). The SPM motor is skewed by 30 mechanical degrees. The general consequence of skewing is to reduce the average torque and power factor, and then output power at high speed. The power of the three motors are compared in Fig. 11, for different skew angles.

The continuous power curves of IM and IPM in the top and medium subfigures of Fig. 11 refer to the nominal skewing. In the same graphs, the effect of twice the skewing angle is also shown, stating that motors with lower slot numbers would suffer more power drop due to skewing effects.

The SPM power curves (bottom of Fig. 11) are not affected by skewing, despite the large skewing angle due to the low number of slots. This counter-intuitive result is justified by the fact that the SPM machine core is quite saturated at no load. The skewed construction results in a machine that is partially less saturated and has nearly the same output characteristics.

In conclusion, skewing has a relatively little impact on the power characteristics of all three motors, even if as a consequence of very different physical reasons.



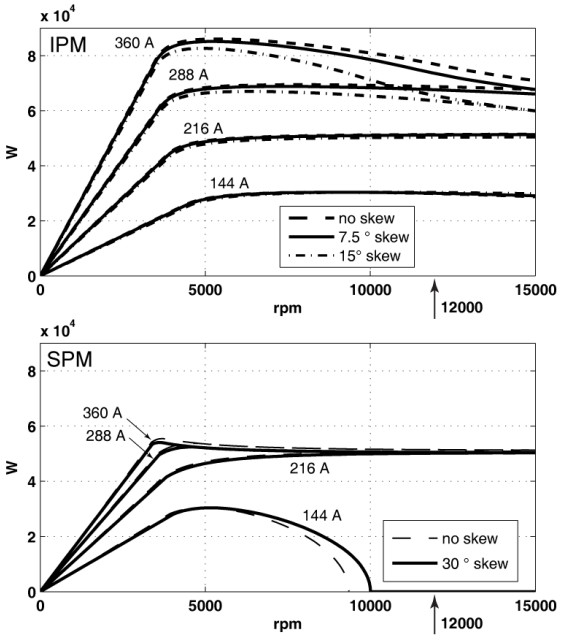
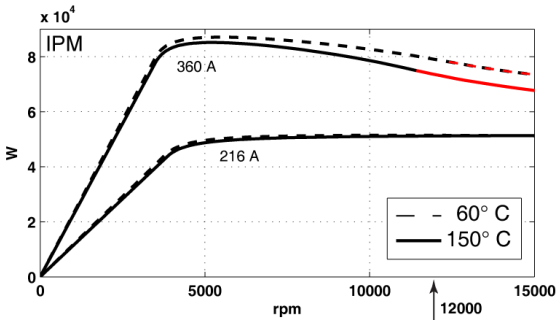


Figure 11. Effect of skewing on the power curves at constant current and voltage of the three design examples.

D. *Effect of rotor temperature*

PM temperature is another factor that affects the power curves of PM synchronous motors. In Fig. 12, the operating temperature of 150°C is compared to the lower value of 60°C. The SPM overload curve (bottom subfigure) is higher at lower temperature due to the higher i_{ch} in (15), given that the characteristic current varies with temperature as the no load flux, according to (8). The IPM motor (top subfigure) is less sensitive to temperature variations than SPM one, as expected from a very salient machine with respect to a non salient one. In particular, the IPM power curve at rated current is practically insensitive to temperature, while the overload curve reduces more evidently at high speed. The rotor temperature of the IM has a very little effect on the output power curves of the example motor and they have not been reported in Fig. 12 for space reasons. E.g. at 3500 rpm, 100 Nm the slip speed is 112 rpm at 20°C and 184 rpm at 180°C.



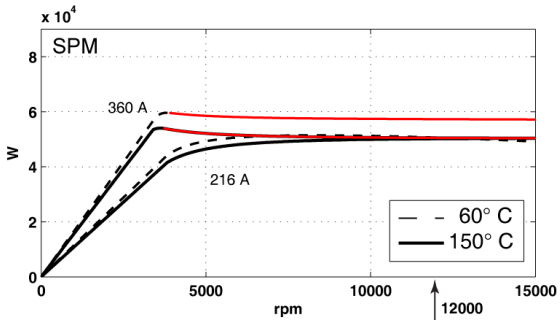


Figure 12. Effect of PM temperature on the power curves of the IPM and SPM motor designs.

VII. LOSS ANALYSIS AND EFFICIENCY

Core losses, PM losses and rotor cage losses of the IM are FEA evaluated with Infolytica Magnet 7.2, via *Transient with motion*, two-dimensional (2D) simulations.

A. *FEA evaluation of core losses*

Core losses are calculated in post-processing by means of a modified Steinmetz equation (16) fitting the manufacturers loss data as a function of flux-density and frequency:

$$\frac{W}{kg} = k_h \cdot f^{\alpha} \cdot B^{\beta} + k_e \cdot f^2 \cdot B^2 \qquad (16)$$

Where the values of the coefficients are: k_h = 0.00778, α = 1.23, β = 1.79, k_e = 3.15e-005 for the for the M250-35A steel grade. The loss model (16) groups the hysteresis and the anomalous loss into a single term, proportional to $(f)^{\alpha}$. The second term of (16), proportional $(f)^2$, accounts for eddy-current loss.

For the SPM and IPM motors, a set of simulations at impressed currents is run on a grid covering the respective operating regions in the (i_d, i_q) plane, at rated speed (4000 rpm). This is very similar to what done for the evaluation of the d, q flux linkages at section VI, and the set of FEA run can even be the same both for fluxes and core losses. The output of the simulations is the loss model at reference speed n_0 = 4000 rpm. The loss model is in the form of four surfaces (modified hysteresis term and eddy current term, both for the stator and the rotor), all four as a function of the current components i_d, i_q. For extrapolating the loss at all speeds, modified hysteresis (h) and the eddy current (e) loss are evaluated in (17) according to the frequency exponents of (16), under the simplifying assumption that the frequency of local flux density variations is proportional to the synchronous speed in all the machine volume:

$$\text{Core loss} = (\text{loss})_h \cdot \left(\frac{n}{n_0}\right)^{\alpha} + (\text{loss})_e \cdot \left(\frac{n}{n_0}\right)^2 \qquad (17)$$

The procedure followed for the IM is similar though the (d, q) stator current components are not known a-priori when

running a current-impressed FEA of an IM. For simulating the willed (i_d, i_q) condition, a current vector of amplitude $\sqrt{i_d^2 + i_q^2}$, rotating at synchronous speed of 4000 rpm is imposed into the motor phases. The rotor speed is set to be constant for having a certain slip speed, that reproduces the (i_d, i_q) condition in rotor-flux synchronous coordinates. The relationship between the slip speed and the RFOC (d, q) current components is known after the static evaluation of the IM magnetic curves introduced at section VI [12]. The extrapolation of stator loss at different speeds is made by (17), where n is the synchronous speed and not the rotor speed in this case. Rotor core loss is negligible with respect to all other loss terms.

B. *FEA evaluation of PM losses*

PM losses are calculated via the same transient with motion FEA simulations used for core loss calculation, throughout all the (i_d, i_q) operating area. The eddy current loss in the solid PM material pieces is calculated by Magnet 2D according to the electrical conductivity of the material, that is 1.5e-006 S/m for the BMH-42SH grade. The PM loss of the example IPM motor turns out to be negligible in all conditions. Dealing with the SPM machine, the loss at different speeds is extrapolated according to the square of the mechanical speed. Tangential segmentation is included in the 2D FEA model, where all magnet poles are made of five segments. Dealing with the effect of axial segmentation, this is evaluated analytically in post-processing [13]: the example motor is segmented in ten pieces axial-wise. Further segmentation in either directions would not give any practical improvement.

C. *FEA evaluation of IM cage losses*

IM cage losses are calculated at any operating point by static FEA, with the rotor resistance estimated analytically [12]. This approach does not account for rotor space harmonics. Therefore, spot transient simulations are run for evaluating the additional rotor cage losses of the IM in specific working points, such as target continuous operation points *F* and *U*, showing that the impact of such loss term is quite limited. Additional losses due to inverter modulation have been FEA calculated and they are under 200 W in all operation modes, at 10 kHz switching frequency, with reference to pulse-width modulation. This loss term will be disregarded in the following.

D. *Power loss maps*

In Fig. 13 the loss maps of the three motors are reported, in the respective torque - speed operating regions. The dashed-line, maximum torque profile in each sub figure represent the current and voltage limits of each motor: as already discussed, this is very limited in the SPM case, while the other two motors show little differences, and only around maximum speed. The other dashed line is representative of the aerodynamic drag, as defined in Fig. 2.

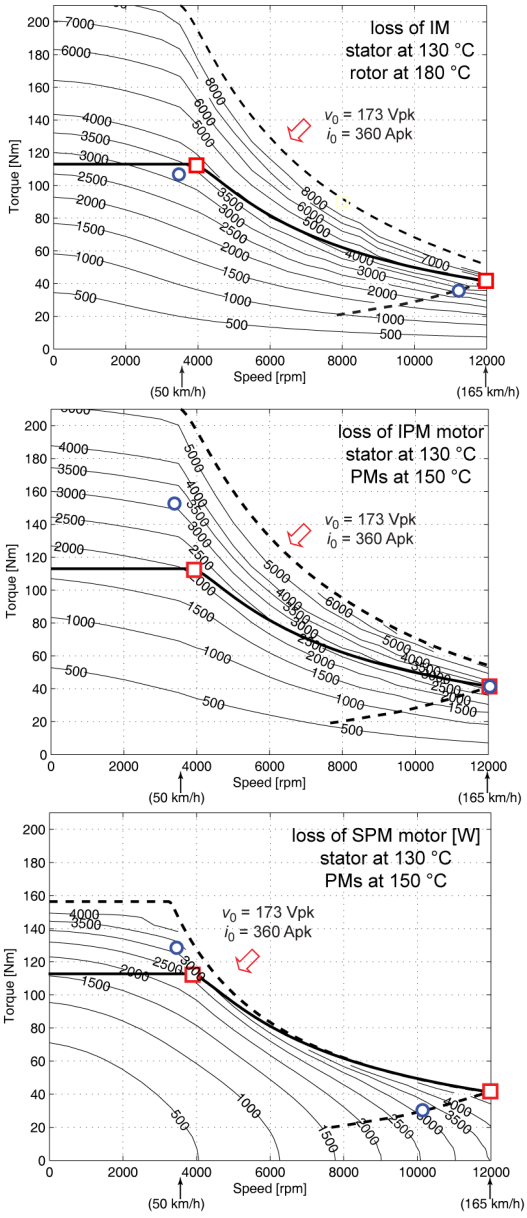


Figure 13. Power loss maps of the three designs over the respective torque versus speed operating regions. The torque limit profiles represent the benchmark continuos operation (continuous line) and the inverter limit (dasehd line).

The IM is the one with the highest losses at low speed. At high speed, it is intermediate between IPM and SPM motors. The SPM is the worst solution at high speed, because of PM loss and Joule loss related to the flux-weakening current component (negative i_d). The IPM motor has the lowest losses in all conditions.

E. *Continuous operation and target points **F** and **U***

The continuous-line torque profile in all sub-plots of Fig.

13, same for all the motors, represents the benchmark of continuous operation. The two reference points ***F*** and ***U***, defined in Fig. 2, are indicated with two square dots. The detail of losses in ***F*** and ***U*** is reported in Fig. 14. The total losses are similar for the two PM machines at low speed (point ***U***), while at high speed SPM is heavily penalized by the PM loss. Stator Joule loss of the SPM are the minimum, due to short end connections. IM ones are the maximum, due to the higher current value for the given specification (as said in subsection VI.A). Stator core loss of the IPM motor is the highest, due to space harmonic fields.

The loss of the IPM motor at rated power point ***F*** is 3200 W, both from Fig. 13b and Fig. 14a. This loss level is now set as a term of comparison between the three motors at high and low speed: the blue circles in Fig. 13 and the horizontal line in Fig. 14 all refer to 3200 W loss. The low speed blue circle is placed at 3650 rpm, corresponding to 50 km/h. The other one is placed on the intersection between the aerodynamic drag curve and the 3200 W curve. Both the circles stand for the ***feasible continuous operation***, in case the common cooling setup coincides with the one designed for the IPM motor.

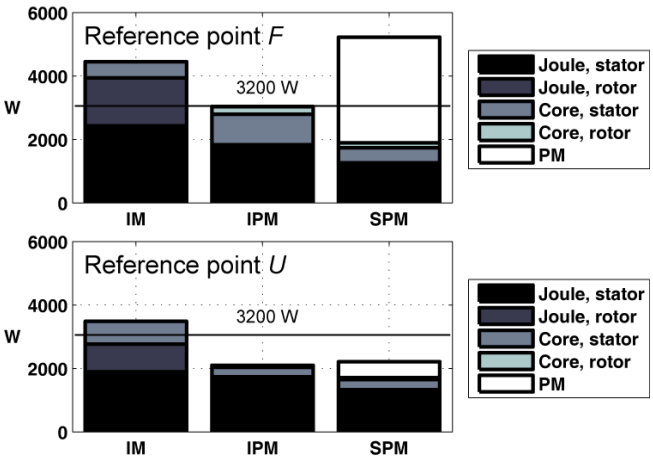


Figure 14. Loss detail in the referece points defined in Fig. 2: a) point *F* is 39 Nm, 12000 rpm; b) point *U* is 110 Nm, 4000 rpm.

The high speed circle of the IPM motor (Fig. 13b) coincides with the target point ***F***, by definition, and the other one is at 155 Nm, well over the torque of the target point ***U***. Dealing with the IM (Fig. 13a), the two circles put in evidence that this is slightly under target both at low and high speed, due to rotor losses. The SPM motor (Fig. 13c) behaves well at low speed and has problems at high speed: at 50 km/h the continuous torque is over U, still with a torque that is lower than the one of the IPM motor, for the reasons described at section V and in [5]. High speed operation would be limited, under the 3200 W loss assumption, to 10300 rpm, due to the very high PM loss (see Fig. 14a), despite the axial and tangential segmentation of the magnets. The feasible continuous operation is the one referred to in Table I, indicated with starred values.

F. *Feasibility of the cooling setup*

The IPM loss of 3200 W corresponds to a specific heat removal of 26 kW/m^2, with reference to the outer surface of the stator stack: 216 mm diameter, 170 mm length, that is 0.115 m^2. This is supposed to be a special cooling setup, out of industrial standard for electric motors.

An example of experimental cooling setup is the one reported in [19], for a prototype motor for hybrid electric traction, with a target speed of 14000 rpm. The liquid cooling has the same flow rate considered here (10 liters per minute) and a higher inlet temperature (105 °C), related to the combustion engine coolant temperature. The prototype of [19] is stopped at 7500 rpm for temperature limits, with a specific heat flow of 19 kW/m^2. The target speed of 14000 rpm would require something like 56 kW/m^2.

Thanks to the lower inlet liquid temperature (60 °C), possible in a purely electric vehicle, the cooling target of 26 kW/m^2 may be considered realistic. Of course, the trend of having very dense motors in traction, with high speed ratings, requires the cooling setups to be designed purposely.

G. *NEDC driving cycle*

The three motors are compared in terms of energy consumption, with reference to the New European Driving Cycle (NEDC), that consists of four repeated ECE-15 driving cycles and an Extra-Urban driving cycle (EUDC) [23]. The vehicle data are reported in the Appendix.

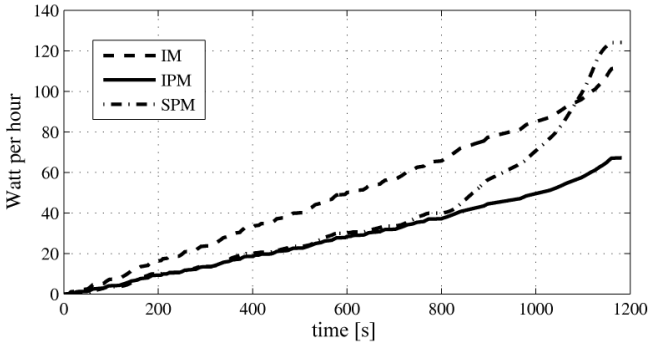


Figure 15. Energy loss over the NEDC driving cycle, for the three motors.

The results, in W per hour, are reported in Fig. 15, and refer to regenerative braking conditions. Motor loss only are considered here: the other loss components of the powertrain, that are those of the battery and the power converters, are out of this comparison. IPM and SPM motors are very similar in the first part of the cycle, referring to urban operation. In sub-urban operation (from time 800 s on) the higher vehicle speed penalizes the SPM. The IM has definitely higher loss than the IPM one, but both motors have a constant rate of energy consumption all over the cycle time: more frequent starts and

stops in urban areas (0 to 800 s) produce the same power loss than less frequent speed variations at higher vehicle speed (800 s to 1200 s).

H. *Efficiency maps*

In Fig. 16 the efficiency maps are reported, giving better evidence of the NEDC results, and of the loss impact in the different areas: the areas corresponding to the urban and sub-urban (ECE15) and extra-urban (EUDC) sections of the NEDC cycle are evidenced by dashed squares. The efficiency in the ECE15 area of IPM and SPM are comparable, as also demonstrated in Fig. 15, between 0 and 800s, and they are both higher than the efficiency of the IM. The EUDC covers the respective high efficiency areas of the IM and the IPM motor, the latter being better than the former, while the efficiency of the SPM motor drops significantly in this area due to speed related losses.

VIII. DISCUSSION

The comparison of the three motor designs leads to the following considerations:

- Both the SPM and IPM motors give the rated 50 kW at 12000 rpm for the same current level (216 A), that is close to the respective characteristic currents. The power curves of the two motors are practically identical at this current level (Fig. 9).
- The SPM motor has no power overload, at higher current levels (Fig. 10).
- Also overload torque is very limited, because at current overload the armature flux heavily saturates the machine core (Fig. 10, low speed region).
- The PM loss at high speed are very high, despite of magnets segmentation and the low number of pole pairs.
- As a consequence, the maximum vehicle speed in continuous operation should be de-rated by a factor 10200 rpm to 12000 rpm, if the same heat dissipation is considered for the SPM and the IPM competitor (Fig. 13, bottom, blue circle).
- Dealing with the IPM motor, the good performance is a consequence of the 48 slots stator, four layers rotor design- This produces a high saliency, resulting in the good overload capability, and an optimal torque versus harmonic loss compromise. Machines with less rotor layers might behave like the low saliency motor of Fig. 6, while machines with lower numbers of stator and rotor slots might incur into less indulgent harmonic loss at high speed [14].

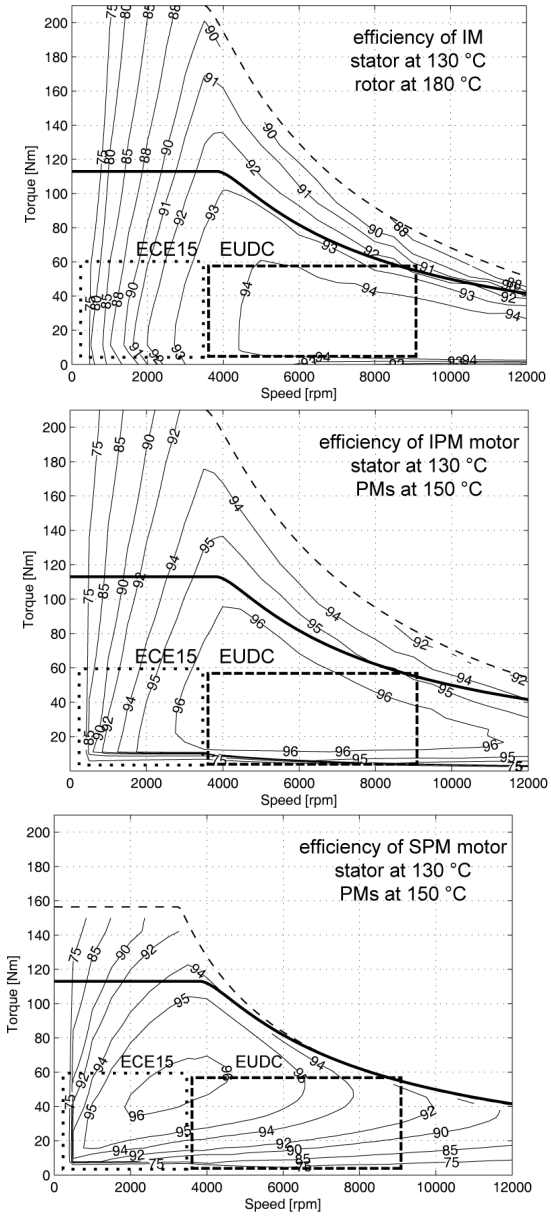


Figure 16. Efficiency maps of the three designs.

- The IM needs more current for giving the rated 50 kW at 12000 rpm (Fig. 9), due to the lower power factor.
- The lower power factor also implies a higher stator current for fulfilling the continuous operation point ***F*:** in Fig. 14, top diagram, the stator Joule loss of the IM is higher than the one of the IPM with the same stator, due to the power factor.
- Moreover, the IM motor is penalized, with respect to the IPM motor, by the cage losses (Fig. 14).
- Nevertheless, the IM has a very good overload capability: at low speed the torque at maximum inverter current is the same as the one IPM motor (Fig. 10, point A').

IX. CONCLUSION

The performance of three AC motor drives for electric traction is compared. The three design examples have the same stack and inverter size and the same cooling. The three designs are FEA evaluated, and all main aspects of magnetic and loss modeling are accounted for.

The SPM motor has severe limitations at overload, independently of the available inverter current, and at high speed, due to PM loss.

The IPM motor has the better overall performance, in terms of power overload curve and efficiency at any load and any speed, provided that it is a high saliency machine, maximized by proper design.

The IM has overload power curves that are not far from the ones of the IPM, provided that is designed to have the lowest possible transient reactance. In terms of loss and energy consumption, this is penalized by the cage losses both at low and high speed.

All considered, the example motors show that it is not always true that SPM machines are more compact and more torque dense than any other machine.

APPENDIX

The vehicle data used for evaluating the NEDC cycle in section VII are reported in Table II.

TABLE II– VEHICLE SPECIFICATION

Vehicle mass	kg	1064
Wheels inertia	$kg \cdot m^2$	2.8
Motor + transmission inertia	$kg \cdot m^2$	0.02
Wheel radius	m	0.285
Frontal area	m^2	1.8
Drag coefficient		0.39
Rolling coefficient	$(km/h)^{-1}$	$3.3 \cdot 10^{-5}$
Static friction coefficient		0.0116
Motor to wheel speed ratio		7.8
Transmission efficiency		0.94
Max vehicle speed	km/h	165

REFERENCES

[1] Zhu, Z.Q.; Howe, D.; "Electrical Machines and Drives for Electric, Hybrid, and Fuel Cell Vehicles," Proceedings of the IEEE, vol.95, no.4, pp.746-765, April 2007

[2] Chau, K.T.; Chan, C.C.; Chunhua Liu; "Overview of Permanent-Magnet Brushless Drives for Electric and Hybrid Electric Vehicles," Industrial Electronics, IEEE Transactions on, vol.55, no.6, pp.2246-2257, June 2008

[3] El-Refaie, A.M.; Jahns, T.M., "Comparison of synchronous PM machine types for wide constant-power speed range operation," Industry Applications Conference, 2005. Fourtieth IAS Annual Meeting. Conference Record of the 2005 , vol.2, no., pp. 1015-1022 Vol. 2, 2-6 Oct. 2005.

[4] EL-Refaie, A.M.; Jahns, T.M., "Optimal flux weakening in surface PM machines using fractional-slot concentrated windings," *Industry Applications, IEEE Transactions on* , vol.41, no.3, pp. 790-800, May-June 2005

[5] Pellegrino, G.; Vagati, A.; Guglielmi, P.; Boazzo, B.; "Performance Comparison Between Surface-Mounted and Interior PM Motor Drives for Electric Vehicle Application," Industrial Electronics, IEEE Transactions on , vol.59, no.2, pp.803-811, Feb. 2012

[6] Jahns, T.M.; Caliskan, V.; "Uncontrolled generator operation of interior PM synchronous machines following high-speed inverter shutdown," *Industry Applications, IEEE Transactions on* , vol.35, no.6, pp.1347-1357, Nov/Dec 1999

[7] PeiZhe Xue; JinFu Lin; "Discussion on the Rare earth resources and its development potential of Inner Mongolia of China," Materials for Renewable Energy & Environment (ICMREE), 2011 International Conference on , vol.1, no., pp.9-12, 20-22 May 2011

[8] Guglielmi, P.; Boazzo, B.; Armando, E.; Pellegrino, G.; Vagati, A.; "Magnet minimization in IPM-PMASR motor design for wide speed range application," Energy Conversion Congress and Exposition (ECCE), 2011 IEEE , vol., no., pp.4201-4207, 17-22 Sept. 2011

[9] Ooi, S.; Morimoto, S.; Sanada, M.; Inoue, Y.; "Performance evaluation of a high power density PMASynRM with ferrite magnets," Energy Conversion Congress and Exposition (ECCE), 2011 IEEE , vol., no., pp.4195-4200, 17-22 Sept. 2011

[10] Soong, W.L.; Miller, T.J.E.; "Field-weakening performance of brushless synchronous AC motor drives" Electric Power Applications, IEE Proceedings, vol.141, no.6, pp.331-340, Nov 1994

[11] Boglietti, A.; Cavagnino, A.; Lazzari, M.; "Computational Algorithms for Induction-Motor Equivalent Circuit Parameter Determination—Part I: Resistances and Leakage Reactances, "Industrial Electronics, IEEE Transactions on , vol.58, no.9, pp.3723-3733, Sept. 2011

[12] Alberti, L.; Bianchi, N.; Bolognani, S.; "Variable-Speed Induction Machine Performance Computed Using Finite-Element," Industry Applications, IEEE Transactions on , vol.47, no.2, pp.789-797, March-April 2011

[13] Sergeant, P.; Van den Bossche, A.; "Segmentation of Magnets to Reduce Losses in Permanent-Magnet Synchronous Machines," Magnetics, IEEE Transactions on , vol.44, no.11, pp.4409-4412, Nov. 2008

[14] Pellegrino, G.; Guglielmi, P.; Vagati, A.; Villata, F.; "Core Losses and Torque Ripple in IPM Machines: Dedicated Modeling and Design Tradeoff," Industry Applications, IEEE Transactions on , vol.46, no.6, pp.2381-2391, Nov.-Dec. 2010

[15] Xu, X.; Novotny, D.W.; "Selection of the flux reference for induction machine drives in the field weakening region," Industry Applications, IEEE Transactions on , vol.28, no.6, pp.1353-1358, Nov/Dec 1992

[16] Sang-Hoon Kim; Seung-Ki Sul; "Maximum torque control of an induction machine in the field weakening region," Industry Applications, IEEE Transactions on , vol.31, no.4, pp.787-794, Jul/Aug 1995

[17] Bianchi, N.; Bolognani, S.; "Unified approach to the analysis and design of an AC motor drive for flux-weakening operations," Industry Applications Conference, 1998. Thirty-Third IAS Annual Meeting. The 1998 IEEE , vol.1, no., pp.95-102 vol.1, 12-15 Oct. 1998

[18] Yamazaki, K.; Shina, M.; Kanou, Y.; Miwa, M.; Hagiwara, J.; "Effect of Eddy Current Loss Reduction by Segmentation of Magnets in Synchronous Motors: Difference Between Interior and Surface Types, "Magnetics, IEEE Transactions on, vol.45, no.10, pp.4756-4759, Oct. 2009

[19] EL-Refaie, A.M.; Alexander, J.P.; Galioto, S.; Shah, M.R.; Kum-Kang Huh; Gerstler, W.D.; Tangudu, J.; Jahns, T.M.; "Scalable, low-cost, high performance IPM Motor for Hybrid Vehicles," Electrical Machines (ICEM), 2010 XIX International Conference on , vol., no., pp.1-6, 6-8 Sept. 2010

[20] El-Refaie, A.; Jahns, T.M.; McCleer, P.J.; McKeever, J.W.; "Experimental verification of optimal flux weakening in surface PM machines using concentrated windings," Industry Applications Conference, 2005. Fourtieth IAS Annual Meeting. Conference Record of the 2005 , vol.2, no., pp. 1050- 1057 Vol. 2, 2-6 Oct. 2005

[21] Gyu-Hong Kang; Jung-Pyo Hong; Gyu-Tak Kim; Jung-Woo Park; , "Improved parameter modeling of interior permanent magnet

synchronous motor based on finite element analysis," Magnetics, IEEE Transactions on , vol.36, no.4, pp.1867-1870, Jul 2000

[22] Yamazaki, K.; Fukushima, N.; , "Experimental validation of iron loss model for rotating machines based on direct eddy current analysis of electrical steel sheets," Electric Machines and Drives Conference, 2009. IEMDC '09. IEEE International , vol., no., pp.851-857, 3-6 May 2009

[23] DieselNet, Emission Test Cycles-Summary of worldwide engine and vehicle test cycles,

URL: http://www.dieselnet.com/standards/cycles/ece_eudc.php

[24] P. Alger, Induction Machines, Their Behavior and Uses, 2nd ed. Paris,

France: Gordon and Breach, 1970.